materials

MDPI

Article

Dependence of Modified Butterworth Van-Dyke Model Parameters and Magnetoimpedance on DC Magnetic Field for Magnetoelectric Composites

Lei Chen [1] and Yao Wang [2,*]

[1] Key Lab of Computer Vision and Intelligent Information System, Chongqing University of Arts and Sciences, Chongqing 402160, China; 20060012@cqwu.edu.cn
[2] School of Electronic Information and Electrical Engineering, Shanghai Jiao Tong University, Shanghai 200240, China
* Correspondence: yaowang898@sjtu.edu.cn

Abstract: This study investigates the impedance curve of magnetoelectric (ME) composites (i.e., $Fe_{80}Si_9B_{11}/Pb(Zr_{0.3}Ti_{0.7})O_3$ laminate) and extracts the modified Butterworth–Van Dyke (MBVD) model's parameters at various direct current (DC) bias magnetic fields H_{dc}. It is interesting to find that both the magnetoimpedance and MBVD model's parameters of ME composite depend on H_{dc}, which is primarily attributed to the dependence of FeSiB's and neighboring PZT's material properties on H_{dc}. On one hand, the delta E effect and magnetostriction of FeSiB result in the change in PZT's dielectric permittivity, leading to the variation in impedance with H_{dc}. On the other hand, the magnetostriction and mechanical energy dissipation of FeSiB as a function of H_{dc} result in the field dependences of the MBVD model's parameters and mechanical quality factor. Furthermore, the influences of piezoelectric and electrode materials properties on the MBVD model's parameters are analyzed. This study plays a guiding role for ME sensor design and its application.

Keywords: magnetostriction; modified Butterworth-Van Dyke model; magnetoimpedance effect; mechanical quality factor; magnetoelectric composite

Citation: Chen, L.; Wang, Y. Dependence of Modified Butterworth Van-Dyke Model Parameters and Magnetoimpedance on DC Magnetic Field for Magnetoelectric Composites. *Materials* **2021**, *14*, 4730. https://doi.org/10.3390/ma14164730

Academic Editor: Franz Faupel

Received: 25 July 2021
Accepted: 16 August 2021
Published: 21 August 2021

1. Introduction

Magnetoelectric (ME) materials produce strong ME effects due to the mechanical coupling between magnetostrictive and piezoelectric materials, which has been studied intensively in both theories and experiments [1–6]. Such ME effects provide a promising candidate for the highly sensitive DC magnetic field sensor due to its significant variations with external direct current (DC) magnetic field. Dong et al. [7] presented a ME laminate under a constant drive of H_{ac} = 1 Oe, which can reach the limit of detection (LOD) for a DC magnetic field H_{dc} of 10^{-4} Oe. Sun et al. [2] reported a novel Nano-Electromechanical System (NEMS) AlN/FeGaB resonator with a high DC magnetic field sensitivity of 280 kHz/Oe and a LOD of 8×10^{-6} Oe. Liu et al. [8] demonstrated a highly sensitive DC magnetic field sensor with a LOD of 2×10^{-5} Oe. Martins et al. [9] showed a Metglas/poly(vinylidene fluoride)/Metglas magnetoelectric laminate with the sensitivity of 30 mV·Oe^{-1} and resolution of 8 μ Oe for H_{dc} detection, and its correlation coefficient, linearity and accuracy values reached 0.995, 95.9% and 99.4%, respectively. Yao et al. [10] developed a Metglas/PMNT/Metglas laminate with the LOD of 10×10^{-5} Oe for H_{dc} detection. Wang et al. [11] also proposed a transformer-type magnetic sensor consisting of soft magnetostrictive alloy FeBSiC/piezoelectric ceramics $Pb(Zr,Ti)O_3$/FeBSiC heterostructure wrapped with both the exciting and sensing coils, which provided the maximum magnetic field sensitivity of 2.12 V/Oe and equivalent magnetic noise of 114×10^{-8} Oe/$\sqrt{HZ}$ (at 1 Hz).

Meanwhile the material property and structure of ME composite have been researched intensively for the magnetic sensor application. As such, the field-dependent characteris-

tics of piezomagnetic coefficient for magnetostrictive material [12], the effect of different magnetostrictive materials on the H_{dc} sensitivity [13–16], and the optimum structure of piezoelectric/magnetostrictive composite [17–20] etc. were reported. Additional to understanding the material property of ME composite, it is essential to study the equivalent electrical parameters of ME composite to further improve the DC magnetic sensor performance. However, few articles have reported and analyzed the H_{dc} dependence of equivalent electrical parameters based on the modified Butterworth–Van Dyke (MBVD) model of magnetoelectric material, even though this is crucial to guide the conditioning circuit design of the ME sensor. Hence, the exploration of electrical equivalent circuit for ME device in this study facilitates understandings of corresponding electrical resonance behavior, which is beneficial for the design and optimization of impedance matching circuits for ME devices. Additionally, this study is expected to guide the design of the magnetic-field-tuned ultrasonic transducer, which can effectively solve the problem of resonance frequency shift and impedance mismatch of the ultrasonic transducer. It is noted that the MBVD model characterizes the loss mechanisms more accurately compared to the conventional Butterworth–Van Dyke model by considering the effects of additional electrical losses and dielectric losses, which can model the measured results more accurately.

In this paper, we investigate the equivalent circuit of the ME sensor based on the MBVD model of PZT/FeSiB laminated composite. It is noted that Lead zirconate titanate $Pb(Zr_{0.3}Ti_{0.7})O_3$ (PZT) exhibits the outstanding piezoelectric performance and high mechanical quality factor compared to other piezoelectric materials such as polyvinylidene fluoride (PVDF) and $BaTiO_3$ etc. Meanwhile, the FeSiB (International standard trademark Metglas-2605 S2) possesses a low saturation field and a strong magnetostrictive effect at low magnetic biases H_{dc} due to its ultrahigh magnetic permeability (i.e., the initial magnetic permeability of 45,000). Correspondingly, magnetostrictive material FeSiB and piezoelectric material PZT are utilized for the ME composite in order to obtain highly magnetic sensing capabilities. In this study, the electrical equivalent circuit parameters of the ME sensor are calculated with the electrical resonance characteristics of measured impedance. Furthermore, the dependences of magnetoimpedance and corresponding MBVD model's parameters on DC magnetic field are measured and discussed. Such dependences are mainly attributed to the delta E and magnetostrictive effects of FeSiB and correspondingly varied PZT's dielectric permittivity. Additionally, the effects of the piezoelectric materials and electrode material's properties on the MBVD model's parameters are analyzed. The study of electrical equivalent circuit facilitates the understanding of electrical resonance behavior for ME devices, and it plays a crucial role in the design of impedance matching circuits for ME devices. Meanwhile, the controllable impedance and dielectric permittivity of PZT/FeSiB ME composites with DC bias magnetic field have broad potential applications, such as tunable spin filters, storage devices, and magnetic sensor etc.

2. Experiment

The ME sensor consists of PZT/FeSiB laminated composite, where the sizes of magnetostrictive (FeSiB, supplied by Foshan Huaxin Microlite Metal Co., Ltd., Foshan, China) layer and the piezoelectric (PZT, produced by Zibo Yuhai Ceracomp Co., Ltd., Zibo, China) layer are 12 mm × 5 mm × 0.03 mm and 12 mm × 6 mm × 0.8 mm, respectively. First, the PZT plate and FeSiB ribbon are dipped in organic impregnant to clean them. Subsequently, the soft magnetic ribbon FeSiB is bonded with PZT plate by using epoxy glue. Here the West System 105/206 resin/hardener epoxy with a good mechanical property and a low viscosity is utilized to provide strong bondings among layers. The mixture ratio for the epoxy part 'Resin' and part 'hardener' is specified as 5:1 by the supplier. Then the PZT/FeSiB laminated composite is compacted in a vacuum bag and cured for 12 h at room temperature to further guarantee the strong bonding among layers. The thickness of the epoxy layers is controlled to be less than 5 μm with vacuum bagging techniques, which has been proved to negligibly affect the ME performance, according to previous research [19]. Considering the ease of fabrication and ME performance, the PZT/FeSiB

laminated composite is designed to operate in the L–T (i.e., longitudinal–transverse) mode. That is to say, the FeSiB layer is magnetized along the longitudinal direction (i.e., length direction) since the demagnetizing field is much smaller along this direction. Meanwhile the silver electrodes of piezoelectric layer are at its top and bottom surfaces, and the PZT is poled along the transverse direction (i.e., thickness direction).

To measure the impedance of ME composite as a function of the external DC magnetic field H_{dc}, H_{dc} is applied along the longitudinal direction of FeSiB layer with a pair of electromagnets driven by a SR830 Lock-In Amplifier. Here the H_{dc} varies from 0 to 400 Oe, which is calibrated with a Gauss magnetometer (Lake Shore 455 DSP, Columbus, OH, USA). Additionally, when analyzing the dielectric characteristics of the ME sensor, an Impedance Analyzer (4194 A HP Agilent, Santa Clara, CA, USA) is used to measure the magnetoimpedance (Z) of ME composite with the excitation frequency ranged from 125 kHz to 155 kHz.

3. Results and Discussion

Figure 1 shows the impedance Z of the ME sensor as a function of electrical excitation frequency f when the varied DC bias magnetic field is applied along the length direction. As illustrated in the inset of Figure 1, the maximum and minimum impedance as a function of excitation frequency show a strong dependence on DC bias magnetic field.

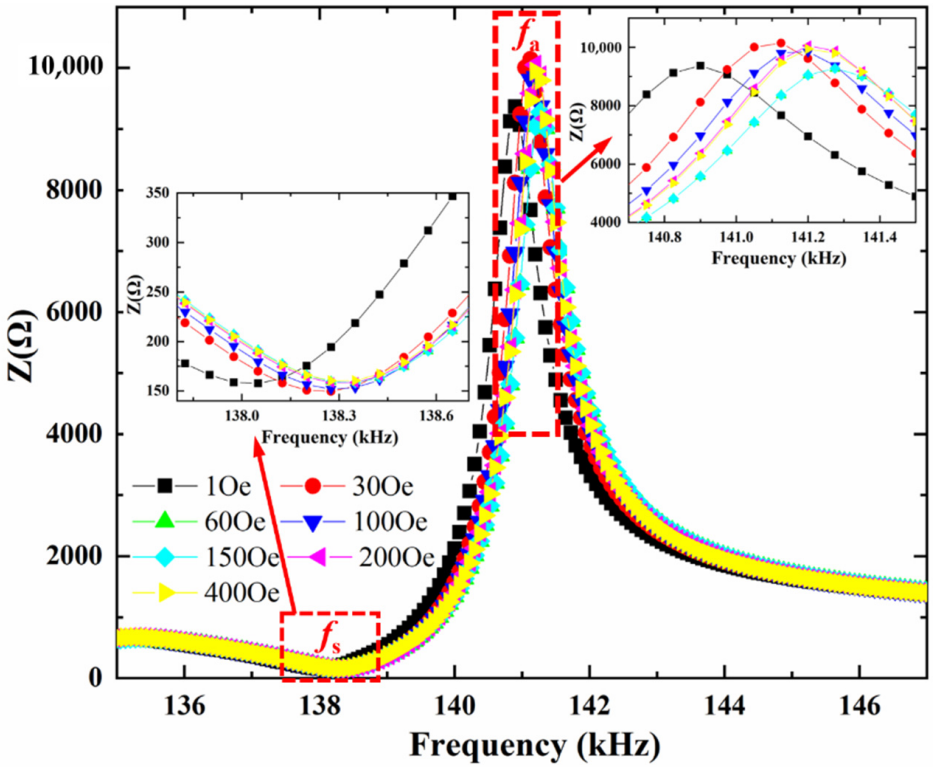

Figure 1. Impedance curve of the ME sensor at various bias DC magnetic fields, and the insets show enlarged details around the maximum and minimum impedances. The maximum relative standard deviations (RSD, i.e., standard deviation/mean × 100%) of impedance with multiple measurements is 0.27%.

It is known that the impedance of the ME sensor is defined by [21],

$$Z = \sqrt{\frac{\mu_0 \mu_{eff}}{\varepsilon_0 \varepsilon_{eff}}} \quad (1)$$

where μ_{eff} and ε_{eff} are the effective relative permeability and permittivity, μ_0 and ε_0 are vacuum permeability and permittivity, respectively. The effective relative permittivity ε_{eff} can be represented as [22].

$$\varepsilon_{eff} = \varepsilon_r + d_{31,p}^2 E_m \left[\frac{n_{pzt} E_{pzt}}{(1 - n_{pzt}) E_m + n_{pzt} E_{pzt}} \frac{\tan\left(\frac{\pi f}{2 f_s}\right)}{\frac{\pi f}{2 f_s}} - 1 \right] \quad (2)$$

where ε_r is relative permittivity of piezoelectric material, $d_{31,p}$ is the piezoelectric coefficient, f_s is the resonance frequency, E_{pzt} and E_m are the Young's modulus of piezoelectric and magnetostrictive materials, respectively. n_{pzt} and $1 - n_{pzt}$ are the volume fractions of piezoelectric material PZT and magnetostrictive material FeSiB in the ME sensor, respectively.

By applying a DC bias magnetic field to the magnetostrictive material FeSiB, the magnetostriction is produced by FeSiB and transferred to the PZT layer through interfacial coupling. Meanwhile the magnetostrictive stress will also change the Young's modulus E_m of magnetostrictive material FeSiB and corresponding resonance frequency f_s. Correspondingly from the inset of Figure 1, the electromechanical resonance frequency f_s of the ME sensor shows a strong dependence on DC bias magnetic field H_{dc}. Specifically, the resonance frequency f_s of the ME sensor is determined by the geometrical dimensions and material parameters (i.e., Young's modulus and mass density) of both piezomagnetic and piezoelectric materials, and is expressed as [12],

$$f_s = \frac{1}{2l} \sqrt{\frac{\overline{E}}{\overline{\rho}}} \quad (3)$$

where l is the length of the ME sensor, $\overline{\rho}$ and $\overline{E}$ are the average density and equivalent Young's modulus of ME laminate, respectively. For the ME composite, $\overline{E}$ and $\overline{\rho}$ are determined by [6],

$$\overline{E} = (1 - n_{pzt}) E_m + n_{pzt} E_{pzt} \quad (4)$$

$$\overline{\rho} = (1 - n_{pzt}) \rho_m + n_{pzt} \rho_{pzt} \quad (5)$$

where ρ_{pzt} and ρ_m are the densities of piezoelectric and magnetostrictive materials, respectively.

Here the Young's modulus of magnetostrictive material FeSiB is given by [23],

$$E_m = \frac{\sigma}{s^e + s^{me}} \quad (6)$$

where s^e, σ, s^{me} are the elastic strain, elastic stress and magnetoelastic strain, respectively. The magnetoelastic strain arises from the magnetic domain reorientation during the varied H_{dc} [24,25], which results in the change in effective Young's modulus with H_{dc}. As a result, the shifts in corresponding resonance frequency (Equation (3)) with H_{dc} are observed.

According to Equations (1) and (2), the variations in the Young's modulus E_m of FeSiB and resonance frequency f_s with H_{dc} also lead to the changes in effective relative permittivity and corresponding impedance with H_{dc} for ME composite. It is noted that the combination of magnetoresistance (MR) and the Maxwell–Wagner effect could also cause the magnetodielectric effect, according to the previous report [26]. However, for our asymmetric PZT/FeSiB laminate, piezoelectric material PZT is covered with the insulating epoxy glue at surface to prevent the current penetrating into the neighboring magnetic ribbon FeSiB. Hence, there is no giant magnetoresistance effect since the sensing current cannot go through the magnetic layers and, correspondingly, no spin dependent scattering phenomenon happens in the ferromagnetic layer. Furthermore, Castel et al. [22] have also reported that the magnetodielectric effect of $BaTiO_3$-Ni laminated composite could reach 10% near the resonance frequency at H_{dc} = 6 kOe and clarified that the magnetodielectric mechanism of their composites was based on the strain effect instead of the Maxwell—Wagner effect.

It is also interesting to find in Figure 2 that the maximum impedance Z_m at the antiresonance frequency (f_a) increases to a maximum value at H_{dc} = 30 Oe, and then decreases with further increasing H_{dc}, while the minimum impedance Z_n at the resonance frequency (f_s) varies in the opposite trend. Namely, Z_n decreases to a minimum value, and then increases with the increasing H_{dc}. This is mainly because the capacitance is directly proportional to dielectric permittivity, the minimum capacitance value at f_a results in the maximum impedance Z_m and the maximum capacitance value at f_s leads to the minimum impedance Z_n according to Equation (1).

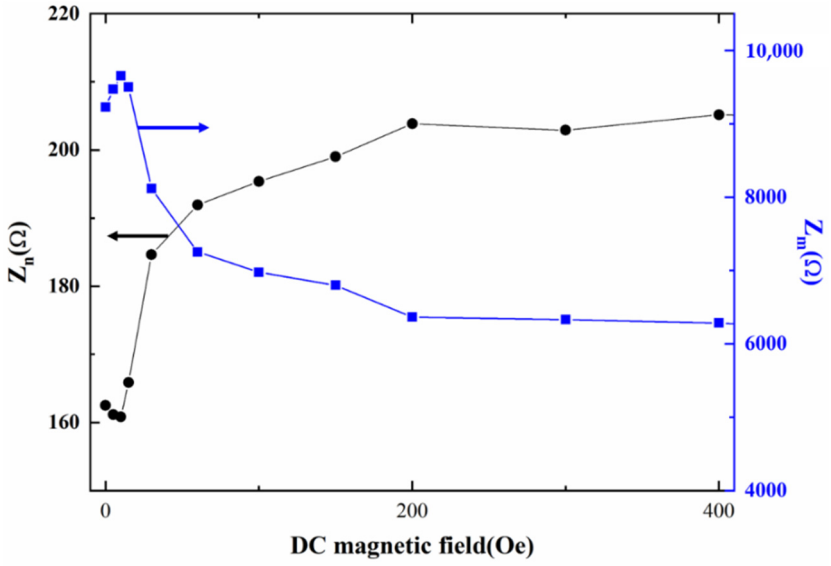

Figure 2. The maximum impedance Z_m and minimum impedance Z_n as a function of DC magnetic field. The maximum RSDs of maximum impedance and minimum impedance with multiple measurements are 0.24% and 0.25%, respectively.

In order to understand the trend of impedance as a function of *DC* magnetic field, the electromechanical (ME) sensor is characterized with a lumped-parameter equivalent circuit based on the MBVD model, as shown in Figure 3. To characterize the loss from the electrodes, the MBVD model adds two additional loss resistors (i.e., R_0 and R_s) to obtain a more accurate model compared with the standard Butterworth–Van Dyke model. It consists of two network branches in parallel, where R_0 represents the resistance associated with dielectric losses of the ME sensor, R_s represents the resistance associated with electrical losses of electrode, R_m denotes the resistance associated with mechanical losses, L_m and C_m denote the motional inductance and capacitance, C_0 represents the static capacitance formed between top and bottom electrodes of the ME sensor.

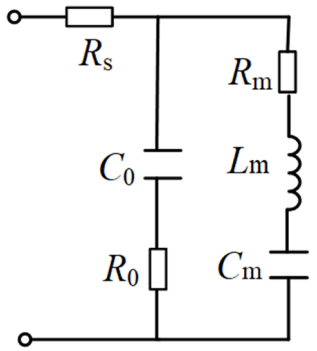

Figure 3. The modified Butterworth–Van Dyke (MBVD) circuit for the ME sensor.

The analytical expression of impedance $Z(\omega)$ and the electrical admittance $Y(\omega)$ for MBVD model are given by [27,28],

$$Z(\omega) = R_s + \frac{(R_0 + \frac{1}{j\omega C_0})(R_m + \frac{1}{j\omega C_m} + j\omega L_m)}{R_0 + \frac{1}{j\omega C_0} + R_m + \frac{1}{j\omega C_m} + j\omega L_m} \quad (7)$$

$$Y(\omega) = \frac{1}{\frac{1}{R_m + \frac{1}{j\omega C_m} + j\omega L_m} + \frac{1}{\frac{1}{j\omega C_0} + R_0}} + R_s \quad (8)$$

The series resonance frequency f_s and antiresonance frequency f_a can be expressed as [27,28],

$$f_s = \frac{1}{2\pi\sqrt{L_m C_m}} \quad (9)$$

$$f_a = \frac{1}{2\pi}\sqrt{\frac{C_m + C_0}{C_0 L_m C_m}} = f_s\sqrt{\frac{C_m + C_0}{C_0}} \quad (10)$$

Using Equations (7), (9) and (10), the model parameter values of C_0, R_0, R_s, L_m, C_m and R_m are extracted from the measured Z. Table 1 lists all the extracted model parameters. To verify the MBVD model for further design of the conditioning circuit, the simulation of the model is implemented with the electrical simulator Agilent ADS. Figure 4 presents the computed impedance Z and phase based on the extracted model parameters at H_{dc} = 30 Oe, which shows a good agreement with the measured data.

Table 1. Parameters of the equivalent circuit model for ME resonator at H_{dc} of 30 Oe.

Model Parameters	R_m	L_m	C_m	R_0	R_s	C_0
values	88.3 Ω	30.2 mH	43.8 pF	20.8 Ω	60 Ω	1.08 nF

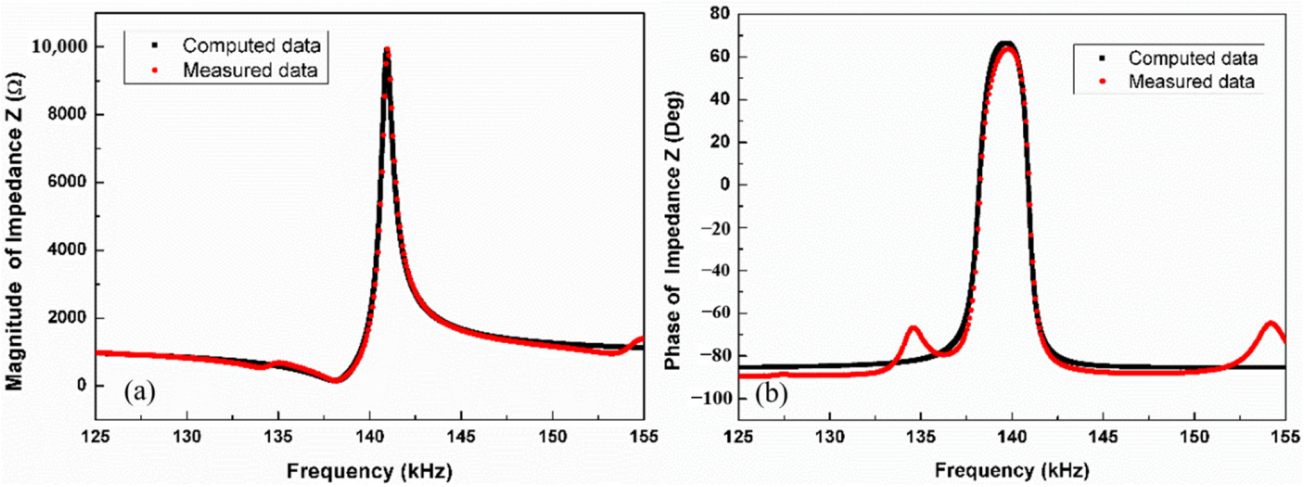

Figure 4. The (**a**) impedance and (**b**) phase angle of the ME sensor as a function of the electrical excitation frequencies ranged from 125 kHz to 155 kHz at H_{dc} = 30 Oe. The maximum RSDs of measured impedances and phase angles are 0.21% and 0.23%, respectively.

According to the measured Z with DC bias magnetic field H_{dc}, the corresponding equivalent circuit parameters (i.e., C_m, L_m, C_0, Q_s, $R_s + R_m$, f_s and f_a) are calculated and analyzed as a function of H_{dc}, as shown in Figures 5–8, respectively.

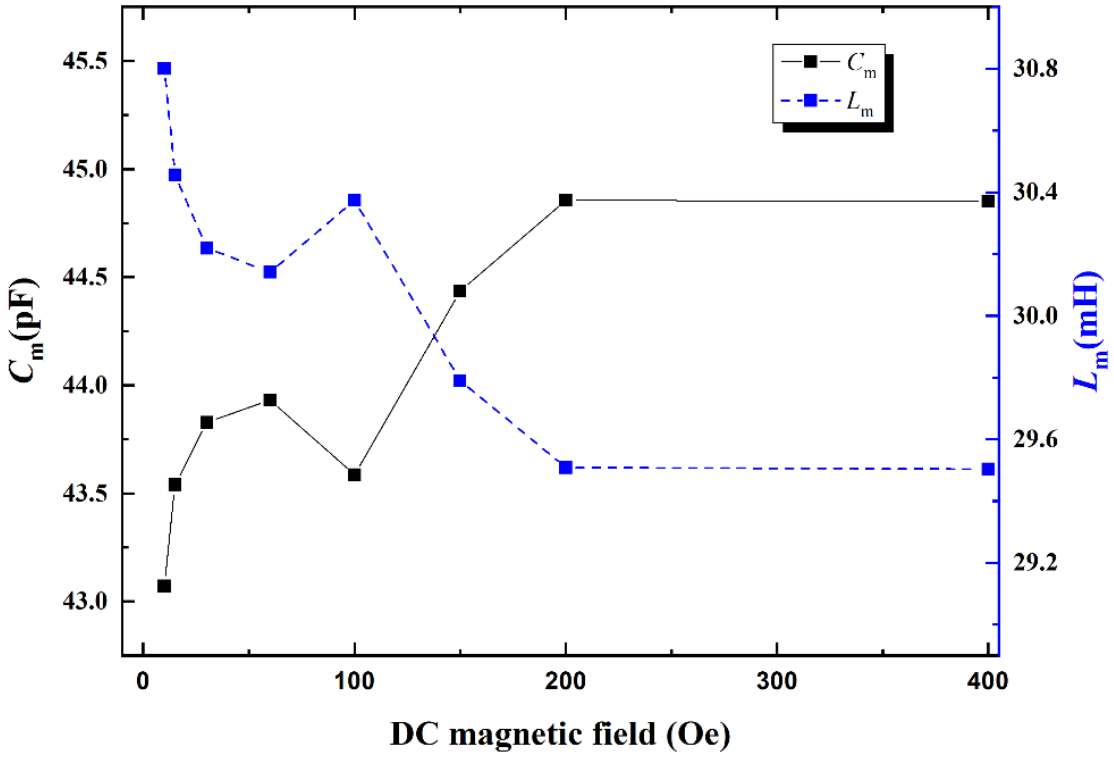

Figure 5. The C_m and L_m of the ME sensor as a function of DC magnetic field. Here, the maximum RSDs of C_m and L_m with multiple measurements are 0.23% and 0.25%, respectively.

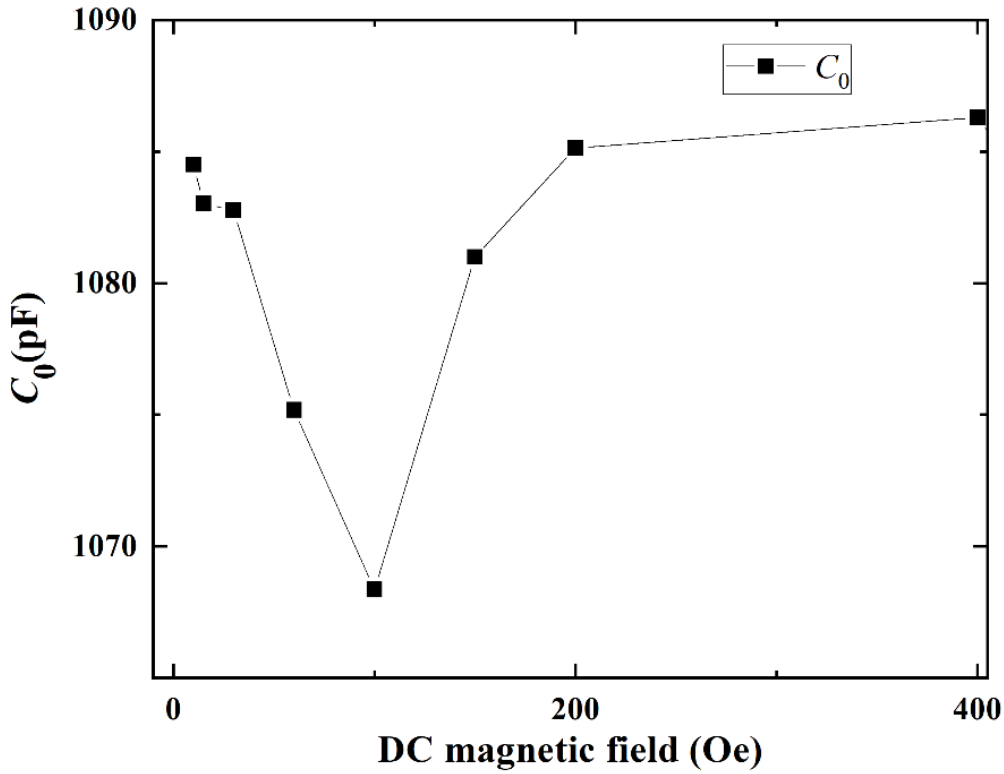

Figure 6. C_0 of the ME sensor as function of DC magnetic field. The maximum RSD of C_0 with multiple measurements is 0.25%.

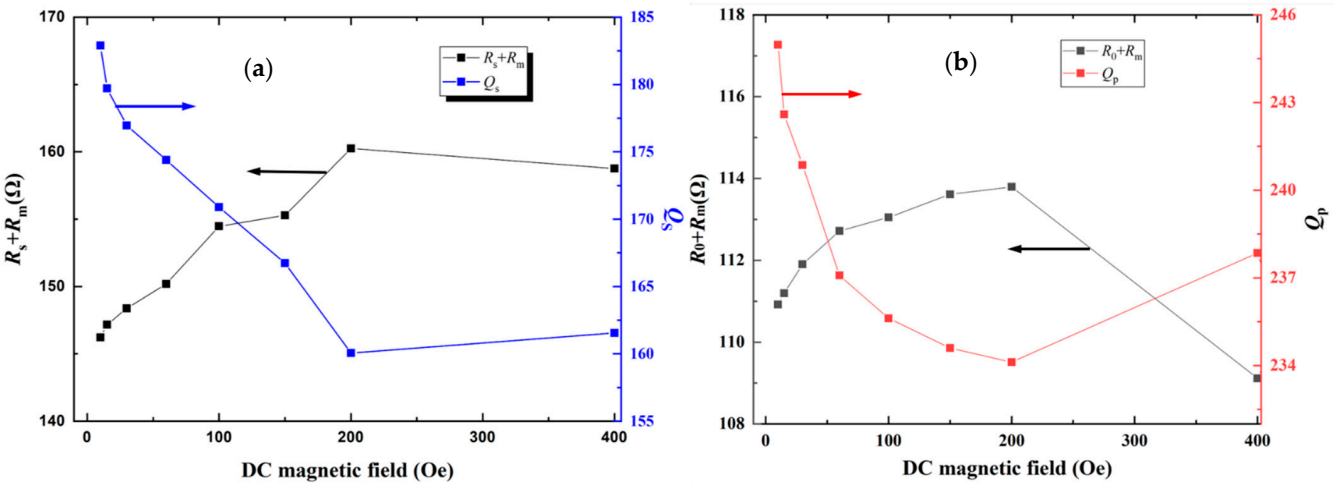

Figure 7. (**a**) The Q_s and $R_s + R_m$ of the ME sensor as a function of DC magnetic field; (**b**) The Q_p and $R_0 + R_m$ of the ME sensor as a function of DC magnetic field. The maximum RSDs of Q_s and Q_p with multiple measurements are 0.22% and 0.21%, respectively. The maximum RSDs of $R_s + R_m$ and $R_0 + R_m$ with multiple measurements are 0.24% and 0.26%, respectively.

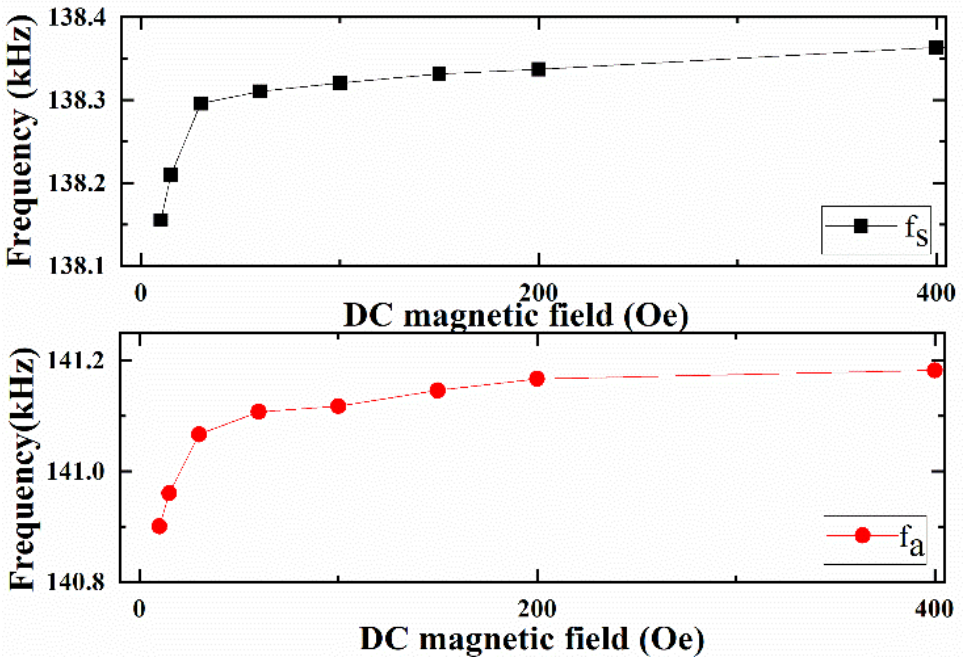

Figure 8. Resonance frequency f_s and antiresonance frequency f_a of ME resonator as a function of DC magnetic field. The maximum RSDs of f_s and f_a with multiple measurements are 0.23% and 0.27%, respectively.

Specifically, C_m and L_m are given by [27,28],

$$L_m = \frac{1}{8}\frac{\rho A l_t}{l_w^2}\left(\frac{s_{11}^E}{d_{31}}\right)^2 = \frac{1}{8}\frac{\rho l l_t}{l_w}\left(\frac{s_{11}^E}{d_{31}}\right)^2 \tag{11}$$

$$C_m = \frac{8}{\pi}\frac{A}{l_t}\frac{d_{31}^2}{s_{11}^E} = \frac{8}{\pi}\frac{l l_w}{l_t}\frac{d_{31}^2}{s_{11}^E} \tag{12}$$

where d_{31}, s_{11}^E, ρ, l_w, l_t and l are the piezoelectric coefficient, elastic compliance coefficient, density, width, thickness and length of the ME sensor, respectively. $A = l l_w$ is the plate area.

It is obvious that the the length l and elastic compliance coefficient s_{11}^E have strong influences on the C_m and L_m according to Equations (11) and (12). Specifically, due to the stress-strain coupling of interlayers, the magnetostrictive strain produced by FeSiB under varying H_{dc} results in the change in the length l and elastic compliance coefficient s_{11}^E for piezoelectric material. As a result, the equivalent electrical parameters C_m and L_m of the ME sensor strongly depend on H_{dc} and vary in the opposite ways, as illustrated in Figure 5. This is due to the fact that L_m and C_m are proportional to $\left(\frac{s_{11}^E}{d_{31}}\right)^2$ and $\frac{d_{31}^2}{s_{11}^E}$, respectively.

Furthermore, C_m is proportional to the length l of composite, whereas it is inverse proportional to the elastic compliance coefficient. Since the Young's modulus is the inverse of elastic compliance coefficient, C_m is determined by both the Young's modulus E and length l. On one hand due to the stress-strain coupling of the interlayers, the length l increases quickly to a maximum value due to the large piezomagnetic coefficient $d_{33,m}$ of FeSiB and then l reaches the saturation with further increasing H_{dc}. On the other hand, the Young's modulus E of the magnetostrictive layer and, corresponding, ME composite decrease initially to a minimum value with the increasing H_{dc}, and then increases and reaches saturation at large H_{dc} when H_{dc} further increases [18]. When H_{dc} < 60 Oe, the magnetostriction does not attain to saturation, C_m is affected by both Young's modulus and the length l. However, the effect of length l on C_m is more obvious than that of Young's modulus due to the large $d_{33,m}$ of FeSiB at the small H_{dc}, which causes C_m to increase with H_{dc} and reach a positive peak in low magnetic field H_{dc} = 60 Oe. When H_{dc} further increases above 60 Oe, the magnetostriction reaches saturation quickly; however, the Young's modulus E still varies significantly and plays a dominant role in C_m. Currently, Young's modulus E and corresponding C_m reach the local minimum values when H_{dc} further increases to 100 Oe, then C_m gradually increases and reaches saturation with further increasing H_{dc} due to the variation in E, as shown in Figure 5.

Meanwhile the static capacitance C_0 can be also expressed with the following expressions [28]:

$$C_0 = \frac{A\varepsilon_r\varepsilon_0}{l_t} \tag{13}$$

where ε_r and ε_0 are the relative dielectric permittivity and vacuum permittivity of the piezoelectric material, respectively.

When H_{dc} is applied along the longitudinal direction of the ME sensor, the magnetostrictive material FeSiB expands with the increasing H_{dc}, which changes dielectric permittivity of piezoelectric material due to the transferred magnetostrictive stress. Correspondingly, C_0 varies with the DC magnetic field since C_0 is strongly determined by the dielectric permittivity. Yao et al. [10] reported that the dielectric permittivity of Terfenol-D/PZT magnetoelectric composite at the resonant frequency decreased and then increased with increasing dc magnetic field. In this case, C_0 varies in a similar trend as function of H_{dc} since C_0 is proportional to the dielectric permittivity. Specifically, it is shown in Figure 6 that the static capacitance C_0 of the ME sensor first decreases with the increasing H_{dc}, and then gradually increases.

The R_m is used to characterize the mechanical loss, which is subject to energy loss in the ME sensor. It can be given as [28],

$$R_m = \frac{l_t^3}{8Ad_{31}^2} = \frac{l_t^3}{8ll_wd_{31}^2} \tag{14}$$

R_m is primarily determined by the length l. Correspondingly, the variations in the length l due to the magnetostriction of FeSiB cause the variation in R_m with H_{dc}.

By analyzing the variation in equivalent circuit parameters (i.e., C_m, L_m, C_0, R_m etc.) with H_{dc}, it is found that the varying magnetostrictive strain of FeSiB with H_{dc} is the main reason for the H_{dc} dependences of equivalent circuit parameters. Furthermore, it is also noted that these equivalent circuit parameters depend on the actively vibrating area A,

since R_m and L_m decrease with the enlarged area, whereas the capacitances C_0 and C_m increase with the enlarged area. Such relations are important for designing ME sensors.

Furthermore, the mechanical Quality factor (Q-factor) reflects the capability of the ME sensor to reserve mechanical energy and the corresponding loss of resonant circuit. Q is defined as the ratio of the stored energy to the dissipated energy per cycle during oscillation. According to Lakin's method, the Q_s at series resonance frequency f_s and Q_p at antiresonance frequency f_a can be defined as [27,28],

$$Q_s = \frac{2\pi f_s L_m}{R_s + R_m} \tag{15}$$

$$Q_p = \frac{2\pi f_p L_m}{R_0 + R_m} \tag{16}$$

On one hand, the smaller value of R_S is desired to improve the effective mechanical Quality factor Q_s of the ME sensor, according to Equation (15). Since R_S represents the electrical loss of electrode, the type and quality of the electrode materials directly affect the Q_s of the ME sensor. In this case, utilizing the electrode material with high acoustic impedance and low resistivity can reduce R_S and improve the effective electromechanical coupling coefficient of the ME sensor. On the other hand, Equation (16) predicts that the high Q_p value can be obtained when the ME sensor possesses a low R_0. Since the dielectric losses R_0 of the ME sensor is mainly determined by the dielectric loss of piezoelectric material, it means the smaller dielectric loss results in the larger effective mechanical Quality factor Q_p of the ME sensor. Additionally, from Equations (15) and (16), it is found that both Q_s at resonance frequency and Q_p at antiresonance frequency decrease with the increasing mechanical loss R_m. Hence, the mechanical loss R_m plays a primary role in the energy dissipations of the ME sensor.

Subsequently, the Q_s, Q_p and corresponding loss as a function of H_{dc} are experimentally investigated to verify and further understand the above theoretical analysis. It is known that R_m depends on the mechanical energy dissipation $tan\delta_{mech}$ of the ME sensor [28], while Q_s is inversely proportional to $tan\delta_{mech}$ [29]. When the DC magnetic field is applied, the mechanical energy dissipation $R_s + R_m$ of magnetostrictive material FeSiB changes dramatically owing to the non-180° domain wall motions. This results in the varied mechanical quality factor Q_s of the ME sensor with H_{dc}, as shown in Figure 7a. Specifically, the quality factor (Q_s) at the series resonance frequency f_s decreases from 182 to the minimum value of 160 at the H_{dc} = 200 Oe and then gradually increases according to the MBVD model. Obviously, the variation in Q_s is mainly attributed to the magnetic mechanical loss associated with magnetic domain wall movement and material damping of FeSiB.

Furthermore, the trends of Q_p and $R_0 + R_m$ as a function of H_{dc} are similar to that of Q_s and $R_s + R_m$, as shown in Figure 7b. However, the magnitude of antiresonance mechanical quality factor Q_p ranges from 234 to 245.6, which is higher than the resonance mechanical quality factor Q_s. The differences between Q_p and Q_s were also reported by in previous literature [30,31]. Finally, the resonance frequency f_s and antiresonance frequency f_a of ME laminated sensor as a function of varied H_{dc} are investigated, as shown in Figure 8. Both f_{s} and f_{a} exhibit similar trends with H_{dc}, which increases with the increasing DC bias field. The obvious shifts of resonance frequency f_s and antiresonance frequency f_a with H_{dc} indicate that f_s and f_a of the ME sensor are adjustable by varying the DC bias magnetic field.

4. Conclusions

In summary, the impedance of the ME sensor (i.e., FeSiB/PZT composite) as a function of DC bias magnetic field is experimentally measured and theoretically analyzed. Meanwhile, the simulation results with the MBVD model of the ME sensor agrees with the measured impedance Z accurately. Specifically, the dependences of extracted MBVD model parameters and the magnetoimpedance effects of the ME sensor on H_{dc} are observed, which result from the varied magnetostriction and the mechanical energy dissipation of

magnetostrictive material FeSiB with H_{dc} due to the corresponding delta E effect and magnetostrictive effect. Furthermore, the influences of piezoelectric materials property and electrode on the MBVD model parameters are analyzed. The analysis of MBVD model for ME composite is beneficial to the design of analog front-end circuits for the corresponding magnetic sensor, which could further improve the LOD.

Author Contributions: Y.W. designed the project; L.C. developed ME composite and carried out experimental works, L.C. carried out simulation work; all authors analyzed the data and reviewed the manuscript; L.C. and Y.W. wrote the paper; L.C. funding acquisition. All authors have read and agreed to the published version of the manuscript.

Funding: This research is supported by the National Natural Science Foundation of China (Grant No. 61304255), and the Scientific and Technological Research Program of Chongqing Municipal Education Commission (No. KJZD-K201901301), and the Natural Science Foundation of Chongqing (No.cstc2020jcyj-msxmX0899), and Key projects of technological innovation and application demonstration in Chongqing (Grant No. cstc2018jszx-cyzdX0175).

Institutional Review Board Statement: Not applicable.

Informed Consent Statement: Not applicable.

Data Availability Statement: Data sharing is not applicable to this article.

Conflicts of Interest: The authors declare no conflict of interest.

References

1. Rupp, T.; Truong, B.D.; Williams, S.; Roundy, S. Magnetoelectric transducer designs for use as wireless power receivers in wearable and implantable applications. *Materials* **2019**, *12*, 512. [CrossRef]
2. Leung, C.M.; Li, J.; Viehland, D.; Zhuang, X. A review on applications of magnetoelectric composites: From heterostructural uncooled magnetic sensors, energy harvesters to highly efficient power converters. *J. Phys. D Appl. Phys.* **2018**, *51*, 263002. [CrossRef]
3. Li, M.; Matyushov, A.; Dong, C.; Chen, H.; Lin, H.; Nan, T.; Qian, Z.; Rinaldi, M.; Lin, Y.; Sun, N.X. Ultra-sensitive NEMS magnetoelectric sensor for picotesla DC magnetic field detection. *Appl. Phys. Lett.* **2017**, *110*, 143510. [CrossRef]
4. Zhang, R.; Zhang, S.; Xu, Y.; Zhou, L.; Liu, F.; Xu, X. Modeling of a magnetoelectric laminate ring using generalized hamilton's principle. *Materials* **2019**, *12*, 1442. [CrossRef] [PubMed]
5. Friedrich, R.M.; Zabel, S.; Galka, A.; Lukat, N.; Wagner, J.M.; Kirchhof, C.; Quandt, E.; McCord, J.; Selhuber-Unkel, C.; Siniatchkin, M.; et al. Magnetic particle mapping using magnetoelectric sensors as an imaging modality. *Sci. Rep.* **2019**, *9*, 1–11. [CrossRef]
6. Spetzler, B.; Kirchhof, C.; Reermann, J.; Durdaut, P.; Höft, M.; Schmidt, G.; Quandt, E.; Faupel, F. Influenceof the quality factor on the signal to noise ratio of magnetoelectric sensors based on the delta-E effect. *Appl. Phys. Lett.* **2019**, *114*, 183504. [CrossRef]
7. Dong, S.X.; Zhai, J.; Xing, Z.; Li, J.F.; Viehland, D. Small dc magnetic field response of magnetoelectric laminate composites. *Appl. Phys. Lett.* **2006**, *88*, 82907. [CrossRef]
8. Dong, X.W.; Wang, B.; Wang, K.F.; Wan, J.G.; Liu, J.M. Ultra-sensitive detection of magnetic field and its direction using bilayer PVDF/Metglas laminate. *Sens. Actuators A Phys.* **2009**, *153*, 64–68. [CrossRef]
9. Reis, S.; Silva, M.P.; Castro, N.; Correia, V.; Martins, P.; Lasheras, A.; Gutierrez, J.; Barandiarán, J.M.; Rocha, J.G.; Lanceros-Mendez, S. Characterization of metglas/poly(vinylidene fluoride)/metglas magnetoelectric laminates for AC/DC magnetic sensor applications. *Mater. Des.* **2016**, *92*, 906–910. [CrossRef]
10. Yao, Y.P.; Hou, Y.; Dong, S.N.; Li, X.G. Giant magnetodielectric effect in Terfenol-D/PZT magnetoelectric laminate composite. *J. Appl. Phys.* **2011**, *110*, 14508. [CrossRef]
11. Wang, Y.; Xiao, N.; Xiao, R.; Wen, Y.; Li, P.; Chen, L.; Ji, X.; Han, T. Enhanced dc magnetic field sensitivity for coupled ac magnetic field and stress driven soft magnetic laminate heterostructure. *IEEE Sens. J.* **2020**, *20*, 14756–14763. [CrossRef]
12. Bian, L.X.; Wen, Y.M.; Li, P. Dynamic magnetomechanical behavior of $Tb_xDy_{1-x}Fe_y$ Alloy under small-signal AC drive fields superposed with various bias fields. *IEEE Trans. Magn.* **2016**, *52*, 1–5. [CrossRef]
13. Chen, L.; Wang, Y. The effects of the soft magnetic alloys' material characteristics on resonant magnetoelectric coupling for magnetostrictive/piezoelectric composites. *Smart Mater. Struct.* **2019**, *28*, 045003. [CrossRef]
14. Chu, Z.; Shi, H.; Shi, W.; Liu, G.; Wu, J.; Yang, J.; Dong, S. Enhanced resonance magnetoelectric coupling in (1-1) connectivity composites. *Adv. Mater.* **2017**, *29*, 1606022. [CrossRef] [PubMed]
15. Lou, G.; Yu, X.; Ban, R. A wide-range DC current sensing method based on disk-type magnetoelectric laminate composite and magnetic concentrator. *Sens. Actuator A Phys.* **2018**, *280*, 535–542. [CrossRef]
16. Huong Giang, D.T.; Tam, H.A.; Ngoc Khanh, V.T.; Vinh, N.T.; Tuan, P.A.; Tuan, N.V.; Ngoc, N.T.; Duc, N.H. Magnetoelectric vortex magnetic field sensors based on the metglas/PZT laminates. *Sensors* **2020**, *20*, 2810. [CrossRef]

17. Zhang, J.; Kang, Y.; Gao, Y.; Weng, G.J. Experimental investigation of the magnetoelectric effect in NdFeB-driven a-line shape terfenol-D/PZT-5A structures. *Materials* **2019**, *12*, 1055. [CrossRef]
18. Li, P.; Wen, Y.M.; Huang, X.; Yang, J.; Wen, J.; Qiu, J.; Zhu, Y.; Yu, M. Wide-bandwidth high-sensitivity magnetoelectric effect of magnetostrictive/piezoelectric composites under adjustable bias voltage. *Sens. Actuators A Phys.* **2013**, *201*, 164–171. [CrossRef]
19. Filippov, D.A.; Galichyan, T.A.; Laletin, V.M. Influence of an interlayer bonding on the magnetoelectric effect in the layered magnetostrictive-piezoelectric structure. *Appl. Phys. A* **2014**, *116*, 2167–2171. [CrossRef]
20. Chu, Z.; Pourhosseiniasl, M.J.; Dong, S. Review of multi-layered magnetoelectric composite materials and devices applications. *J. Phys. D Appl. Phys.* **2018**, *51*, 243001. [CrossRef]
21. Bian, L.X.; Wen, Y.M.; Li, P. Analysis of magneto-mechano-electronic coupling factors in magnetostrictive/piezoelectric laminated composite. *Acta Phys. Sin.* **2009**, *58*, 4205–4213.
22. Israel, C.; Petrov, V.M.; Srinivasan, G.; Mathur, N.D. Magnetically tuned mechanical resonances in magnetoelectric multilayer capacitors. *Appl. Phys. Lett.* **2009**, *95*, 072505. [CrossRef]
23. Cullity, B.D.; Graham, C.D. *Introduction to Magnetic Materials*, 2nd ed.; John Wiley & Sons: Hoboken, NJ, USA, 2009; p. 270.
24. Clark, A.E.; Savage, H.T. Giant magnetically induced changes in the elastic moduli in Tb.3Dy.7Fe2. *IEEE Trans. Sonics Ultrason.* **1975**, *22*, 50–51. [CrossRef]
25. Chen, Z.; Su, Y. The influence of low-level pre-stressing on resonant magnetoelectric coupling in Terfenol-D/PZT/Terfenol-D laminated composite structure. *J. Appl. Phys.* **2014**, *115*, 193906. [CrossRef]
26. Catalan, G. Magnetocapacitance without magnetoelectric coupling. *Appl. Phys. Lett.* **2006**, *88*, 102902. [CrossRef]
27. Luan, G.D.; Zhang, J.D.; Wang, R.Q. *Piezoelectric Transducer and Transducer Array*; Peking University Press: Beijing, China, 2005; p. 114.
28. Buttry, D.A.; Ward, M.D. Measurement of interfacial processes at electrode surfaces with the electrochemical quartz crystal microbalance. *Chem. Rev.* **1992**, *92*, 1355–1379. [CrossRef]
29. Yang, F.; Wen, Y.M.; Li, P.; Zheng, M.; Bian, L.X. Resonant magnetoelectric response of magnetostrictive/piezoelectric laminate composite inconsideration of losses. *Sens. Actuators A Phys.* **2008**, *141*, 129–135. [CrossRef]
30. Zhuang, Y.; Ural, S.O.; Rajapurkar, A.; Tuncdemir, S.; Amin, A.; Uchino, K. Derivation of piezoelectric losses from admittance spectra. *Jpn. J. Appl. Phys.* **2009**, *48*, 041401. [CrossRef]
31. Wang, Y.; Gray, D.; Berry, D.; Gao, J.; Li, M.; Li, J.; Viehland, D. An extremely low equivalent magnetic noise magnetoelectric sensor. *Adv. Mater.* **2011**, *23*, 4111–4114. [CrossRef]